

Lifetime Prediction of DC-Link Capacitors in Multiple Drives System Based on Simplified Analytical Modeling

Haoran Wang¹, Member, IEEE, Shili Huang², Student Member, IEEE, Dinesh Kumar³, Senior Member, IEEE, Qian Wang¹, Member, IEEE, Xiangtian Deng¹, Member, IEEE, Guorong Zhu¹, Senior Member, IEEE, and Huai Wang¹, Senior Member, IEEE

Abstract—Lifetime prediction of dc-link capacitors in a single drive has been discussed before, which indicates that the capacitor in a standard drive meets serious reliability challenges and in a slim drive does not. However, in most of the applications, drives are connected in parallel with the power grid. The large amount of harmonic distortion produced by nonlinearity drives may transmit and couple between grid and drives, which changes the stresses of devices as well as the dc-link filters. Therefore, the estimated results in a single drive cannot be extended to multiple drives any more. This article investigates the lifetime of dc-link capacitors in multiple drives system. First, by decoupling the interactions among grid-connected drives, a simplified equivalent circuit model and its analytical model to obtain the dc-link continuous current in multiple drives is proposed, which releases the designers from configuring the large simulation for multiple drives. Then, applying the lifetime prediction method, the lifetime of dc-link capacitors in multiple drives is investigated, in terms of types of drives, numbers of drives, and grid conditions. The results show that the lifetime of the standard drives extends in the multidrive systems and the lifetime of the slim drives decreases in the multidrive systems, which break the previous mind. Finally, based on the proposed analytical model and lifetime estimation method, the capacitor sizing from reliability aspect for multiple slim drives is given. The outcomes of the lifetime investigation could be a guideline for the design of the capacitive dc link in multidrive systems.

Index Terms—DC-link capacitor, equivalent circuit model, multidrive systems, lifetime.

Manuscript received September 12, 2019; revised February 3, 2020; accepted June 7, 2020. Date of publication June 16, 2020; date of current version September 4, 2020. This work was supported in part by the Innovation Fund Denmark through the Advanced Power Electronic Technology and Tools Project, and in part by project of National Natural Science Foundation of China under Grants 51777146 and 51977163. This paper was presented in part at the IEEE Energy Conversion Congress and Exposition (ECCE), Baltimore, MD, USA, September 29–October 3, 2019, sponsored by Power Electronics Society. Recommended for publication by Associate Editor J. Popovic-Gerber (*Corresponding author: Guorong Zhu*.)

Haoran Wang, Qian Wang, and Huai Wang are with the Department of Energy Technology, Aalborg University, 9220 Aalborg, Denmark (e-mail: hao@et.aau.dk; qiw@et.aau.dk; hwa@et.aau.dk).

Shili Huang, Xiangtian Deng, and Guorong Zhu are with the School of Automation, Wuhan University of Technology, Wuhan 430070, China (e-mail: shili.huang@whut.edu.cn; dengxt@whut.edu.cn; zhgr_55@whut.edu.cn).

Dinesh Kumar is with the Development Center, Danfoss Drives A/S, 6300 Grasten, Denmark (e-mail: dineshr30@ieee.org).

Color versions of one or more of the figures in this article are available online at <https://ieeexplore.ieee.org>.

Digital Object Identifier 10.1109/TPEL.2020.3003236

I. INTRODUCTION

GRID-CONNECTED adjustable speed drives (ASDs) with a front-end diode bridge rectifier is an effective energy saving solution for motors in various industrial, commercial, and residential applications [1], [2]. A dc-link capacitor is an important part of ASDs, which serves to limit the dc-link voltage ripple, absorb harmonics, and provide a certain amount of energy storage for abnormal and transient operations [3], [4]. It contributes high percent of volume, cost, and failure rate in the whole drive [5], [6].

In recent years, reliability of capacitors draws extensive attention [7]–[9]. The failure of these capacitors depends on both the inherent capability of the selected capacitors (e.g., rated voltage, rated current, and rated lifetime) and the operational conditions (e.g., electrothermal stresses) in the field operation [10], [11]. Depending on the structures of ASDs, different dc-link capacitors are implemented. For the standard drives with dc-link *LC* filter, electrolytic capacitors (E-caps) are commonly used due to the cost effectiveness and high energy density [12], [13], [15], [16]. However, the use of E-caps raises the reliability concern. The primary cause of its failure is due to electrolyte evaporation or dielectric material degradation, which highly depends on the electrothermal stresses [17], [18]. High ripple currents cause internal self-heating, increasing the hot-spot temperature, and resulting in aging. Moreover, it increases the equivalent series resistor (ESR) over time [19], [20]. An increase in its ESR causes more heat for a given ripple current, thus increasing the hot-spot temperature rise and accelerating the degradation process. In recent years, slim dc-link drives with significantly smaller dc-link capacitance (i.e., slim drive) implemented by the film capacitor (Film-cap) have been in the market [21], [22]. It benefits the reduction of harmonics and volume, and has potential to improve the reliability. Compared with the E-caps in the standard drives, Film-cap is recognized to be more reliable due to the dry plastic film served as dielectric, which achieves lower ESR and higher current capability.

The lifetime prediction and benchmarking of the capacitors in a standard drive and slim drive have been presented in literatures [23], [24]. The quantitative results are compatible with the theoretical discussion, where the slim drive shows longer lifetime than the standard drive with the same loading

profile [24]. However, in typical applications, drives are not working alone, which are connected in parallel with a low-voltage distribution network in a commercial or an industrial segment [25]. For example, multiple water pumps connected to a step-down transformer, multiple refrigeration and air conditioning in a automation and dairy production, numbers of drives on container ships, and so on [13], [14]. Whether the reliability of dc-link capacitors in multiple drives still keep the same with that in a single drive is the industry's interest and worth to study. The existing research efforts regarding to multidrive systems mainly focus on the power quality of the grid network. The interactions between the power grid and multiple drives may introduce harmonics, which distort the grid current and voltage. Based on the simulation and experimental testing, the total harmonic distortion of the grid current in multiple drives are studied [2]. However, the relationship between the reliability performance and the configurations of drives (e.g., types, numbers, and load conditions) have not been discussed before. The large amount of harmonic distortion produced by nonlinearity drives may transmit and couple between grid and multiple drives, which also changes the stress of the individual dc-link filter. Therefore, the estimated lifetime in a single drive cannot be extended to multiple drives. For the investigation of the lifetime of dc-link capacitors in multidrive systems, following issues need to be addressed with.

- 1) The de-link current causes internal self-heating, which is a key factor of failure. For a single drive, the capacitor current can be obtained from either experimental measurements, simulations, or analytical models by using the time-domain or frequency-domain analysis [25], [26]. Nevertheless, the method cannot be simply scaled up for a system with a large number of drives due to the significantly increased complexity.
- 2) In a multidrive system, the electrothermal stresses and expected lifetime of the dc-link capacitors are altered compared to that of a single drive system. A quantitative analysis of the impact of the number of the drives is missed in the literature for optimal sizing of the capacitors in a multidrive system.

This article investigates the lifetime of the dc-link capacitors in multidrive systems. It aims to find the relationship between the lifetime and the configurations of the multidrive systems in terms of structures, numbers of drive, and grid conditions. The contributions of this article are shown as follows: First, an equivalent circuit model and its analytical model for multidrive systems are proposed to derive the dc-link current of the individual drive. In order to analyze the multidrive systems with both the standard drive and slim drive in different grid conditions, the grid impedance and dc-link filters are considered in the model. To simplify the nonlinear characteristics, the heavy load operating conditions are assumed, where the dc-link current is continuous. Second, applying the lifetime prediction method [1], the lifetime of dc-link capacitors in multidrive systems is investigated comprehensively from the following aspects:

- 1) lifetime benchmarking of dc-link capacitors in both standard drives and slim drives with scalable numbers of drives;

- 2) lifetime benchmarking of dc-link capacitors under different grid conditions in multidrive systems (e.g., standard drives and slim drives);
- 3) lifetime evaluation of dc-link capacitors in a hybrid multidrive system.

Finally, after the lifetime prediction of dc-link capacitors in various configurations and different grid conditions, the impact of the capacitor sizing on the lifetime of dc-link capacitors in multidrive systems is studied. It serves as a guideline for proper selection of configurations of multidrive systems and its parameters to fulfill a certain lifetime requirement.

The rest of this article is organized as follows. In Section II, the overview of the multidrive systems is described. In Section III, an equivalent circuit model and its analytical model for multidrive systems to obtain the dc-link current of an individual drive is presented considering ac-side and dc-side impedance. In Section IV, the lifetime prediction for different configurations of multidrive systems under different grid conditions is investigated; and the capacitor sizing criteria for multidrive systems from the reliability aspect are discussed in Section V. Finally, Section VI concludes this article.

II. OVERVIEW OF A MULTIDRIVE SYSTEMS

The configuration of a single ASD is shown in Fig. 1(a), where the front end of the ASD is a three-phase diode rectifier and the rear end is consist of an inverter. Since the diode rectifier may cause current harmonics due to the nonlinear effects, the dc-link filter is needed to mitigate the harmonics. The widely used harmonic mitigation solution is the standard filter (e.g., LC filter), as shown in Fig. 1(a). The standard filter is implemented with large E-caps C_{dc} and an inductor L_{dc} , where the inductor is used to reduce the line harmonics emissions and the E-caps is used to reduce the fluctuation of the voltage. However, the standard filter is inferior in reliability and volume aspects due to poor reliability of E-caps and the large size of inductor as well as E-caps. Another dc-link filter configuration is a slim filter, as shown in Fig. 1(a), which is implemented with a small Film-cap C_{slim} . The slim filter is well received in the market due to its advantages in cost effectiveness and reliability aspects compared with the standard filter. But actually, in most applications, drives are connected in parallel at the point of common coupling (PCC) instead of a single drive, as shown in Fig. 1(b). The configuration and parameters of multiple drives may be different and the power of the individual drive is vary. The interactions between the power grid and drives will influence the equivalent impedance of the multidrive system, which may significantly affect the electrothermal stress of the individual dc-link capacitor, and further influence the reliability of the dc-link capacitor.

This article focuses on the reliability of the dc-link capacitor in multidrive systems, therefore, the current stress of the capacitor is of great importance, which is mainly determined by the impedance of the ASDs system. The impedance of a single slim drive system is determined by the dc-link slim capacitor and the grid impedance, and the impedance of a single standard filter is determined by the dc-link E-caps, inductor, and grid impedance.

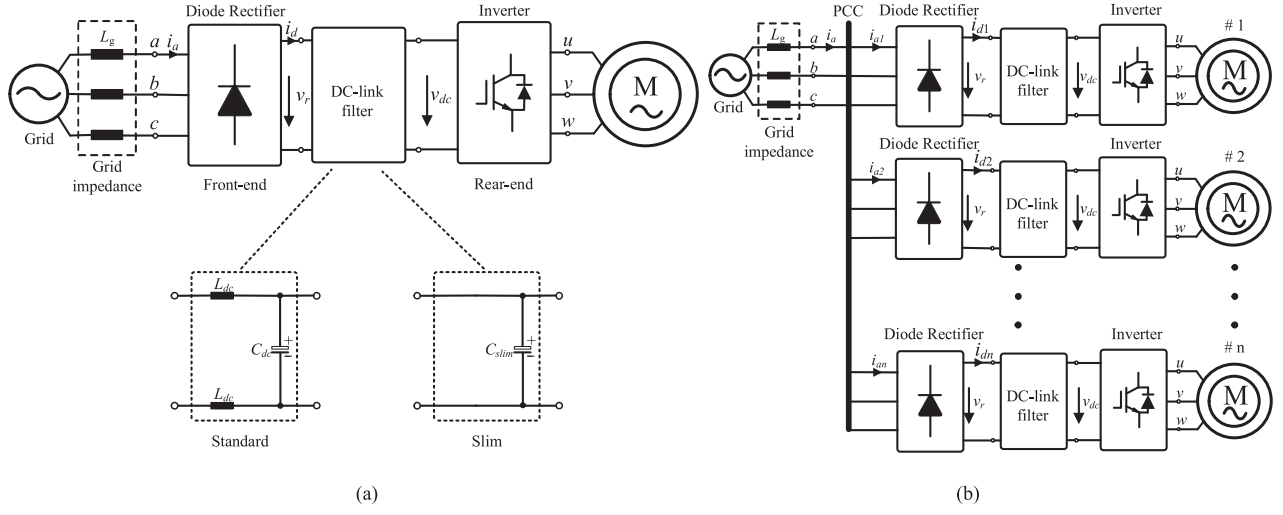


Fig. 1. Block diagram of (a) single ASD system with standard or slim filter configuration and (b) multidrive systems.

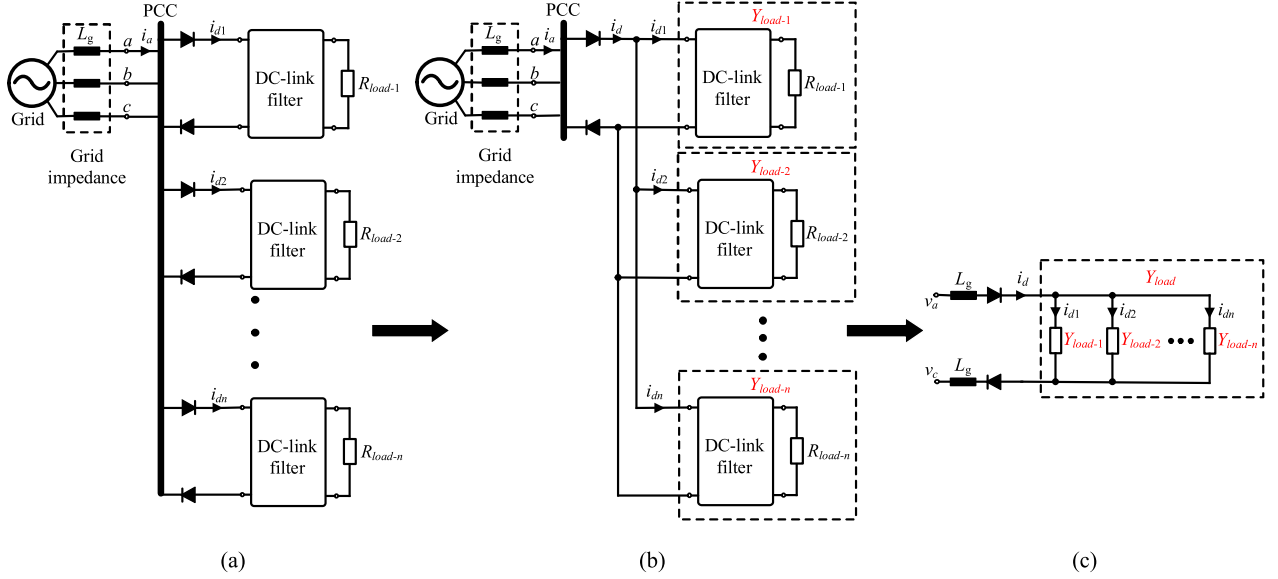


Fig. 2. Block diagram of (a) multidrive systems, (b) simplified model of the multidrive systems, and (c) equivalent circuit model of the multidrive systems.

The grid impedance of the low-voltage distribution network is mainly determined by the size and type of the step-down transformer and feeders. However, for the multiple slim or standard drives system, the grid and drives interact, which influence the impedance of the individual drive. As a result, the impedance of the multiple drives system as well as the reliability of dc-link capacitors depend not only on the grid impedance value and parameters of the drive, but also on the configuration of the other drives connected in parallel.

III. SIMPLIFIED EQUIVALENT CIRCUIT AND ITS ANALYTICAL MODEL

This section studies the simplified equivalent circuit model and the analytical model of multidrive systems. First, the simplified equivalent model of the multidrive system is introduced

considering the interactions among drives. Then, the analytical model to acquire the dc-link capacitor current of the individual drive is provided.

A. Equivalent Circuit Model

When the three-phase diode rectifier is in the conduction period, two of the input voltage sources are connected to the dc link. The interconnection impedance between drives is negligible, the multidrive systems can be simplified in Fig. 2(a) when the diodes are conducting. The load in the simplified equivalent mode is considered as a resistor [i.e., R_{load-k} , $k = (1, 2, \dots, n)$]. Therefore, the multidrive systems in Fig. 2(a) can be simplified in Fig. 2(b). The dc-link filter and the load of each drive can be modeled as an RLC or RC circuit and expressed as an admittance Y_{load-n} . The admittance of multiple drives

connected in parallel can be amalgamate into Y_{load} as shown in Fig. 2(c). As a result, Y_{load} of the equivalent circuit model is given as

$$\begin{aligned} Y_{\text{load}} &= Y_{\text{load-1}} + Y_{\text{load-2}} + \cdots + Y_{\text{load-n}} \\ &= \frac{1}{R_{\text{load}} + jX_{\text{load}}}. \end{aligned} \quad (1)$$

For standard drives

$$Y_{\text{load-n}} = \frac{1 + j\omega C_{\text{dc}} R_{\text{load-n}}}{R_{\text{load-n}} - \omega^2 R_{\text{load-n}} L_{\text{dc}} C_{\text{dc}} + j\omega L_{\text{dc}}}. \quad (2)$$

For slim drives

$$Y_{\text{load-n}} = \frac{1 + j\omega C_{\text{slim}} R_{\text{load-n}}}{R_{\text{load-n}}}. \quad (3)$$

Based on the aforementioned analysis, the multidrive system can be simplified by paralleling the admittance in the dc side. When the type and parameters of drives are the same, multiple admittance paralleled at the dc side can be lumped into an admittance. Then, the current of the dc-link capacitor in a multidrive system can be obtained from one drive, which reduces the complexity.

B. Analytical Model

The equivalent circuit model in Fig. 2(c) enables the analysis of multidrive systems simpler, and it can be described in the analytical model to obtain the dc-link capacitor current stress in multidrive systems. For a balanced three-phase grid

$$\begin{cases} v_a = V_m \sin \theta \\ v_b = V_m \sin(\theta - \frac{2\pi}{3}) \\ v_c = V_m \sin(\theta - \frac{4\pi}{3}) \end{cases} \quad (4)$$

where v_a , v_b , and v_c are instantaneous value of the grid phase voltage, V_m is the amplitude of the grid phase voltage, and θ equals to ωt . The instantaneous dc-side voltage v_r in Fig. 1 can be expressed in terms of the voltage rectifier switching functions S_a , S_b , and S_c

$$v_r = S_a v_a + S_b v_b + S_c v_c. \quad (5)$$

Because the analysis is based on the continuous current mode, the rectifier switching function S_a can be expressed by the Fourier series in (6) [26]. Accordingly, S_b and S_c can be obtained by replacing θ in (6) by $(\theta - 2\pi/3)$ and $(\theta - 4\pi/3)$, respectively

$$\begin{aligned} S_a &= \sum_{q=1,5,7,\dots}^{\infty} \frac{\sqrt{3}}{\pi} \cdot \frac{(-1)^{l+1}}{q} \\ &\times \{\sin qu \cos q\theta - (1 + \cos qu) \sin q\theta\} \end{aligned} \quad (6)$$

where $q = 6l \pm 1$ ($l = 0, 1, 2, \dots, q > 0$), and u is an overlap angle. The overlap angle of multidrive systems can be obtained based on the equivalent circuit model in Fig. 2(c) [26]

$$u = \arccos \left(1 - \frac{2\omega L_g I_d}{\sqrt{3}V_m} \right) \quad (7)$$

where I_d is the dc component of the dc-side current i_d in Fig. 2(c). Substituting (4) and (6) into (5), the dc-side voltage v_r

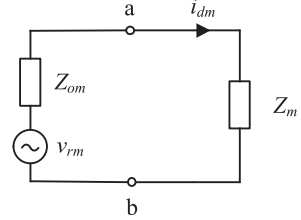


Fig. 3. Equivalent circuit for obtaining harmonic components of the dc current.

is given as

$$\begin{aligned} v_r &= V_r + v_{rm} \\ &= V_r + \sum_{m=6,12,18,\dots}^{\infty} (A_{dm} \cos m\theta + B_{dm} \sin m\theta) \end{aligned} \quad (8)$$

where

$$\begin{aligned} V_r &= \frac{3\sqrt{3}V_m}{2\pi} \{1 + \cos u\} \\ A_{dm} &= \frac{3\sqrt{3}V_m(-1)^p}{2\pi} \left\{ \frac{1 + \cos(m+1)u}{m+1} - \frac{1 + \cos(m-1)u}{m-1} \right\} \\ B_{dm} &= \frac{3\sqrt{3}V_m(-1)^p}{2\pi} \left\{ \frac{\sin(m+1)u}{m+1} - \frac{\sin(m-1)u}{m-1} \right\} \end{aligned}$$

where $m = 6p$ ($p = 1, 2, 3, \dots$).

The dc-side current i_d can be obtained by applying the dc-side voltage v_r and the impedance at the corresponding harmonics frequencies. Based on the equivalent circuit model in Fig. 2(c), the equivalent impedance circuit for obtaining harmonic components of the dc current is shown in Fig. 3. Terminals a and b connect the diode rectifier and the dc-link filter, where Z_m is the m th impedance of the load as viewed from terminals a and b ; Z_{om} is the m th impedance of the ac side, as viewed from terminals a and b , and represents the grid impedance; and v_{rm} is the m th component of the dc-side voltage v_r . From Fig. 2(c), the m th impedance of the load of the multiple drives system is given by

$$Z_m = \frac{1}{Y_{\text{load}}}. \quad (9)$$

The ac-side impedance Z_{om} is not equal to the grid impedance, and it is affected by the overlap angle u , Z_{om} is given by [13]

$$Z_{\text{om}} = j \left(2 - \frac{3u}{2\pi} \right) m\omega L_g. \quad (10)$$

The m th harmonic current component of the dc-side current is

$$i_{dm} = \frac{v_{rm}}{Z_m + Z_{\text{om}}}. \quad (11)$$

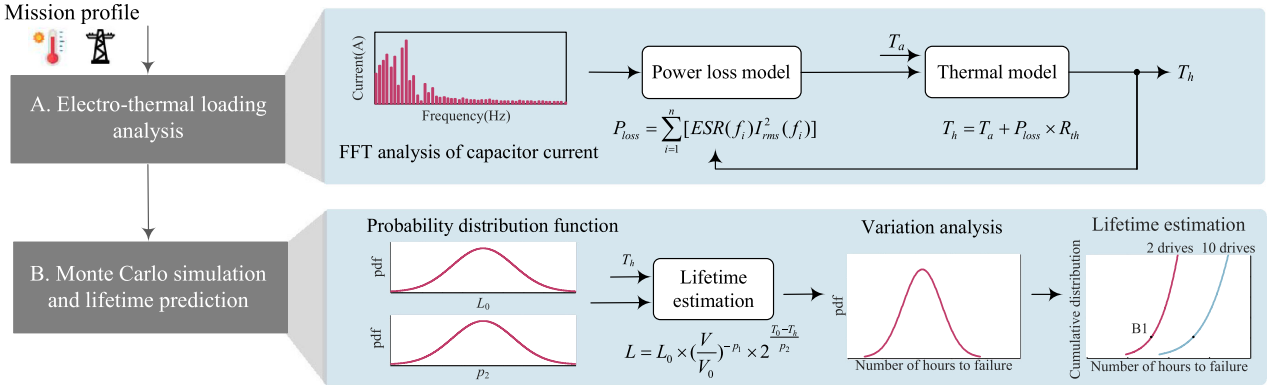


Fig. 4. Lifetime prediction procedure of the dc-link capacitor. ESR(f_i) is the ESR at frequency f_i and $I_{\text{rms}}(f_i)$ is the rms value of the harmonic current at frequency f_i . T_h is the hot-spot temperature and T_a is the ambient temperature, which is 60 °C in this article. R_{th} is the thermal resistance of the capacitor between the hot-spot and ambient. L_0 is the rated lifetime at rated voltage V_0 and temperature T_0 . V is the voltage under operation condition. p_1 is in the range of 7–9.4 for Film-caps, and 3–5 for E-caps based on the existing lifetime model [3]. p_2 is a coefficient assumed to be 10.

Equations (8)–(11) give

$$\begin{aligned} i_d &= I_d + \sum i_{dm} \\ &= I_d + \sum_{m=6,12,18,\dots}^{\infty} \sqrt{2} I_{dm} \cos(m\theta - \beta_m) \end{aligned} \quad (12)$$

where

$$\begin{aligned} I_d &= \frac{V_r}{R_{\text{load}}}, \quad I_{dm} = \frac{\sqrt{(A_{dm}^2 + B_{dm}^2)/2}}{|Z_m + Z_{om}|} \\ \beta_m &= \arctan \frac{B_{dm}}{A_{dm}} + \arctan \frac{Im(Z_m + Z_{om})}{Re(Z_m + Z_{om})}. \end{aligned}$$

The obtained current i_d in (12) is the dc-side current of the equivalent circuit of multidrive systems. Therefore, the dc current of the drive n is

$$\begin{aligned} i_{dn} &= I_{dn} + \sum i_{dn-m} \\ &= i_d \frac{Y_{\text{load}-n}}{Y_{\text{load}}} \end{aligned} \quad (13)$$

where I_{dn} is the dc component of dc-side current of the drive n . The dc-link capacitor current of the individual drive can be obtained from the dc-side current i_{dn} . By analyzing the characteristics of the current shunt, we can get that the harmonic of the dc-side current i_{dn} are absorbed by the dc-link capacitor. Therefore, the dc-link capacitor current equals to the harmonic of the dc-side current, which equals to $\sum i_{dn-m}$.

IV. LIFETIME PREDICTION OF DC-LINK CAPACITORS IN MULTIDRIVE SYSTEMS

This section studies the lifetime prediction of dc-link capacitors in multidrive systems. First, the lifetime prediction method with the proposed capacitor current analytical model is validated step by step. Then, the impact of drives number and the grid conditions on the dc-link capacitor lifetime are investigated. In order to see the impact from different numbers more clearly, the impact from other factors (such as the detail parameters and operating conditions of an individual drive) is minimized.

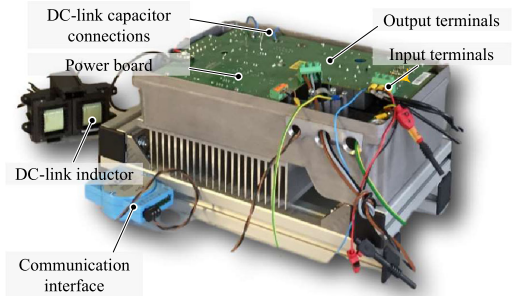


Fig. 5. Experimental prototype of the motor drive with dc-link filter.

Therefore, the operating conditions of each drives are assumed to be the same and the loads are the same resistors, which can be changed for different applications.

A. Lifetime Prediction Method of DC-Link Capacitors

The lifetime prediction procedure of the dc-link capacitor is shown in Fig. 4, which is divided into two parts. The first part is the electrothermal loading analysis, which aims to estimate the hot-spot temperature by using the current stress of the capacitor from different loading conditions. The obtained hot-spot temperature serves as the input of the second part, which is Monte Carlo simulation and lifetime prediction considering the parameters variation in the lifetime model.

The experiment prototype of the motor drive is shown in Fig. 5 and the specification of the ASDs system is shown in Table I. The values of ASDs system specification in Table I are based on commercial products and a real industrial condition, where the values of the standard LC filter and slim capacitor filter are calculated according to the cutoff frequency. Due to the heat dissipation from the diode bridge, dc-link filter, and inverter, the local temperature in the enclosure is defined as 40–60 °C instead of the room temperature. The validation of the equivalent circuit model is implemented in the standard drives system with both soft (i.e., the grid impedance is 130 μH)

TABLE I
SPECIFICATION OF THE ASDS SYSTEM AND THE DC-LINK CAPACITOR CONFIGURATION OF COMMERCIAL PRODUCT

ASDs system specification		Standard LC filter (C_{dc})		Slim capacitor filter (C_{slim})
Rated power (kW)	7.5	Physical configurations	Four 450V/680 μ F electrolytic capacitor	1100V/30 μ F Film capacitor
Grid frequency (Hz)	50	Part number	TDK. B43644A5687M	TDK. B32778G0306
Grid phase RMS voltage (V)	230	ESR of single capacitor	140 m Ω @100Hz	14 m Ω @100Hz
DC-link voltage (V)@7.5kW balanced grid voltage	535	Thermal resistance (R_{th})	6 °C/W	13 °C/W
Grid impedance (L_g)(soft)	130 μ H	Rated load lifetime	5000 hours @105 °C and rated ripple current	100000 hours @70 °C and rated ripple current
Grid impedance (L_g) (stiff)	2 μ H	L_{dc}	1.25 mH	

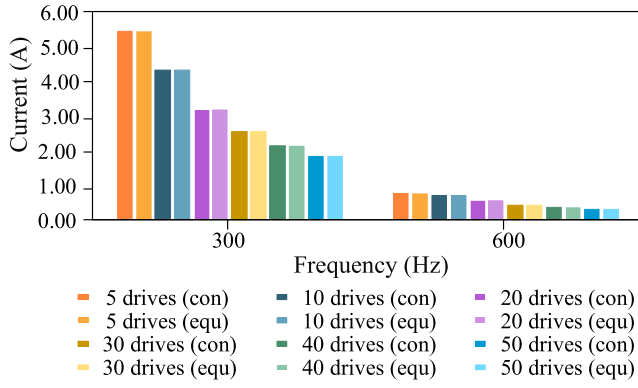


Fig. 6. Comparison between the dc-link capacitor current obtained by the conventional model and equivalent circuit model in a standard drives system under soft grid condition ($L_g = 130 \mu\text{H}$).

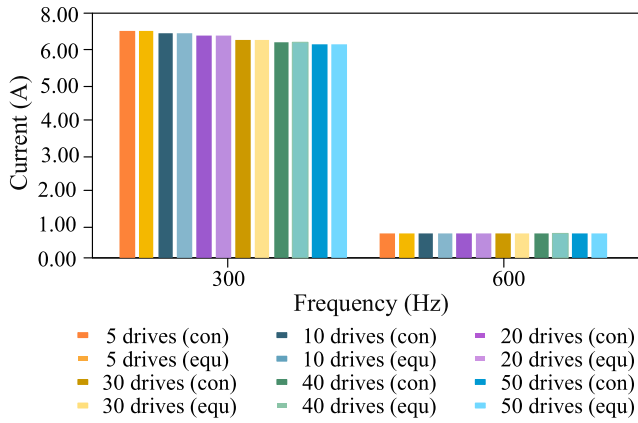


Fig. 7. Comparison between the dc-link capacitor current obtained by the conventional model and equivalent circuit model in a standard drives system under stiff grid condition ($L_g = 2 \mu\text{H}$).

and stiff (i.e., the grid impedance is $2 \mu\text{H}$) grid conditions. The results are shown in Figs. 6 and 7, respectively. It shows that the capacitor current stress obtained by the equivalent circuit model is almost the same with that in the conventional model with numbers of ASDs. The analytical model studied in Section III-B is also validated in the standard drives system with soft and stiff grid conditions, and the results are shown in Figs. 8 and 9, respectively. It shows that the dc-link capacitor current obtained by the proposed analytical model agrees well with that obtained by simulation and the absolute value of difference between is less

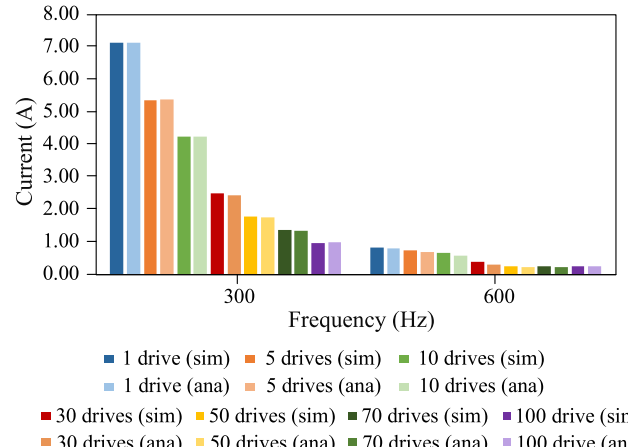


Fig. 8. Comparison between the dc-link capacitor current obtained by the simulation and analytical model in the standard drives system under the soft grid condition ($L_g = 130 \mu\text{H}$).

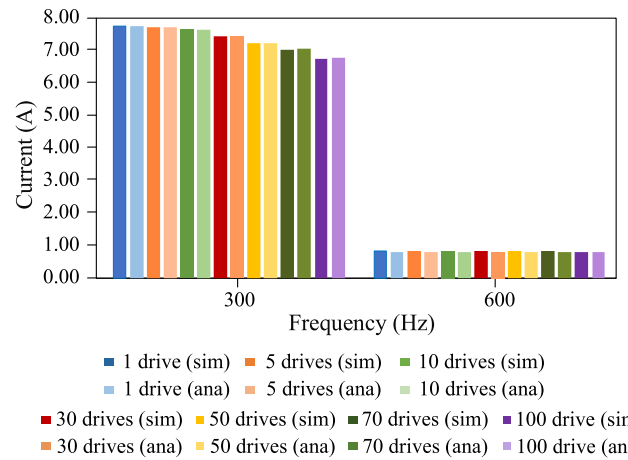


Fig. 9. Comparison between the dc-link capacitor current obtained by simulation and analytical model in the standard drives system under a stiff grid condition ($L_g = 2 \mu\text{H}$).

than 0.1 A. It should be noted that the analytical model applied in this article is suitable for the continuous current mode only, which is important for the lifetime prediction as the heavy load condition will contribute to a higher current stress to the dc-link capacitor.

The hot-spot temperature of the dc-capacitor can be estimated based on its ESR and the harmonic current. The ESR is frequency

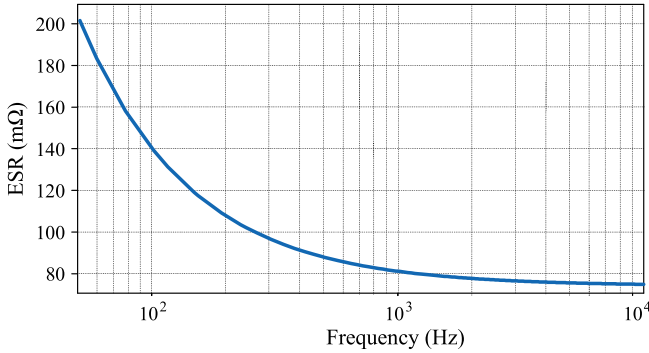


Fig. 10. ESR characteristic curve of E-caps with part number: TDK B43644A5687M.

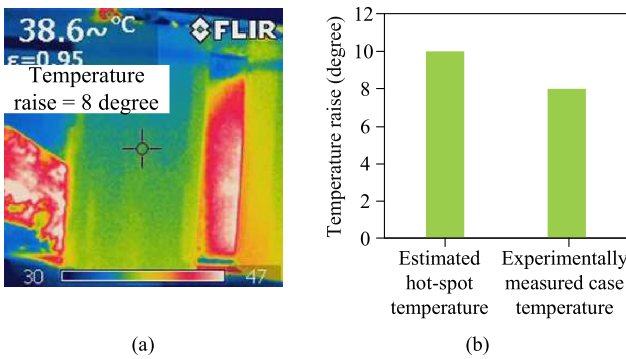


Fig. 11. (a) Tested case temperature in a standard filter under the soft grid condition. (b) Comparison between the experimental and estimated capacitor temperature in a standard filter under the soft grid condition.

dependent. For example, the ESR of E-caps decreases with the higher frequency, which is shown in Fig. 10, however, it is applicable for a certain frequency range, after that, the ESR is increasing due to skin effect.

The hot-spot temperature is given as [1]

$$T_h = T_a + \sum_{i=1}^n R_{th} \times [\text{ESR}(f_i) \times I_{rms}^2(f_i)] \quad (14)$$

where T_h is the hot-spot temperature and T_a is the ambient temperature, which is 60 °C in this article. R_{th} is the thermal resistance of the capacitor between the hot spot and ambient, and the value of it is shown in Table I. $\text{ESR}(f_i)$ is the ESR at frequency f_i and $I_{rms}(f_i)$ is the root mean square (rms) value of the harmonic current at the frequency f_i . The hot-spot temperature of the dc-link capacitor is estimated to be 70 °C based on the thermal model, the ESR characteristic of E-caps, and the capacitor current. The experimentally measured case temperature in the standard filter under the soft grid condition is shown in Fig. 11(a), and the comparison between the experimental and estimated temperature is shown in Fig. 11(b). The case temperature of capacitors is measured because the capacitors in testing setup do not have temperature sensors inside. The difference between the estimated and experimental temperature is about 2° in Fig. 11(b).

The lifetime prediction model used in this article is given as [1]

$$L = L_0 \times \left(\frac{V}{V_0} \right)^{-p_1} \times 2^{\frac{T_0 - T_h}{p_2}} \quad (15)$$

where L_0 is the rated lifetime at the rated voltage V_0 and temperature T_0 . V and T_h are, respectively, the voltage and hot-spot temperature under the operation condition. p_1 is 7–9.4 for the Film-cap, and 3–5 for E-caps. p_2 is a coefficient assumed to be 10 [3].

The following two types of parameter variations are considered in Monte Carlo simulation:

- 1) parameter variations in the applied lifetime prediction model;
- 2) parameter variations due to the difference of manufacturing process among capacitors with the same part number.

For the first type of variation, each lifetime prediction model has its limitations owing to the test conditions, component manufacturing process, and failure mechanism are specific. Therefore, the variation of p_2 is taken into account. For the second type of variation, the variation of L_0 and T_h are taken into account because it has a direct effect on the lifetime of the capacitor. All parameters experience 5% variation with a certain confidence level (e.g., 90%) [1] by means of normal probability distribution functions, as shown in Fig. 12 .

B. Lifetime Prediction of DC-Link Capacitors With Scalable Number of Drives

In typical applications, drives are connected in parallel at the PCC. The interactions between the power grid and multiple drives may influence the electrothermal stress of the individual dc-link capacitor, which will further influence the reliability of the dc-link capacitor. Therefore, the relationship between the reliability of the dc-link capacitor and the number of drives is studied in this article.

The lifetime prediction of the dc-link capacitor is predicted in two types of dc-link configurations, which are standard LC filter and slim capacitor filter. Although the rated power of ASDs is 7.5 kW, the drives operate at partial load conditions in most application. As a result, the ASDs system is considered to operate at 5 kW in this article. It should be noted that the higher rated power of ASDs will contribute to the larger current stress of the dc-link capacitor, and finally, reduce the dc-link capacitor lifetime. The electrical stress of the dc-link capacitor is highly affected by the impedance of ASDs, so the impedance characteristics is of great importance. According to Fig. 2(c) and (1), the impedance of the multiple standard or slim drives system can be acquired as n (the number of ASDs connected in parallel) times of that in a single ASD

$$Z_n = \frac{1}{nY_{load-n}} + 2j\omega L_g. \quad (16)$$

With the impedance characteristics of multiple standard and slim ASDs are shown in Fig. 13(a) and (b), respectively. The following can be observed:

- 1) for the multiple standard drives system, the impedance at 300 Hz increases with more drives connected in parallel,

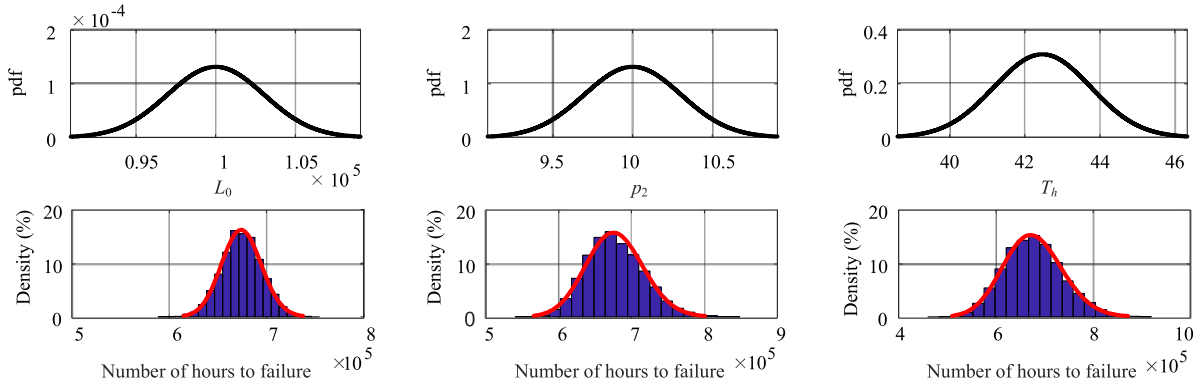


Fig. 12. Probability density functions of the parameters under analysis and lifetime probability distribution function.

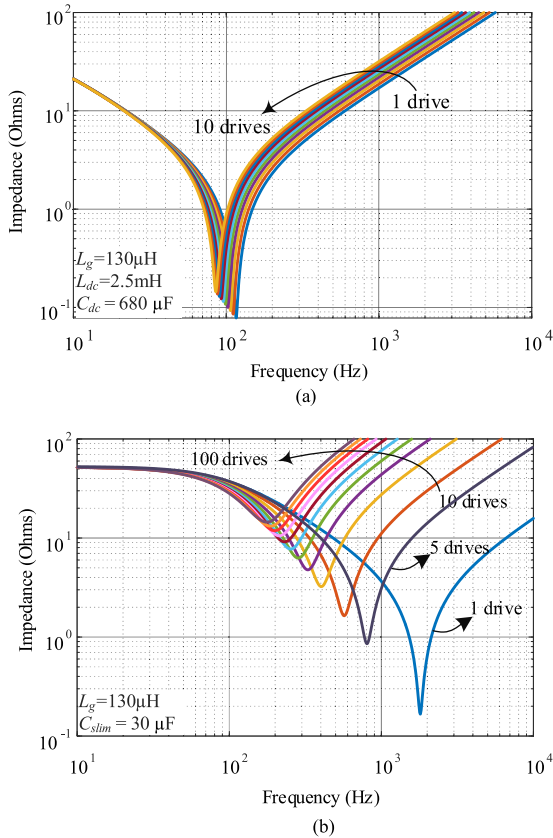


Fig. 13. Impedance characteristics of multiple ASDs system under a soft grid condition ($L_g = 130 \mu\text{H}$). (a) Impedance characteristics of multiple standard ASDs. (b) Impedance characteristics of multiple slim ASDs.

which will result in the decrease in the current of the dc-link capacitor with more standard drives connected in parallel;

- 2) for multiple slim drives system, the impedance at 300 Hz decreases first, and then, increases when the number of drives increases from 1 to 100, so the current stress of the dc-link capacitor increases first, and then, decreases;
- 3) the impedance of the single slim ASD system is the lowest at 1800 Hz, so the current of the dc-link capacitor in a single slim ASD is the highest at this frequency;

- 4) the impedance of the five slim ASDs system is the lowest at 900 Hz, so the current of the dc-link capacitor in five slim ASDs is the highest at this frequency;
- 5) the impedance of the ten slim ASDs system at 600 Hz is the lowest, so the current of the dc-link capacitor in ten slim ASDs is the highest at this frequency;
- 6) the impedance of the 30 slim ASDs system at 300 Hz is the lowest, so the current of the dc-link capacitor in 30 slim ASDs is the highest at this frequency;

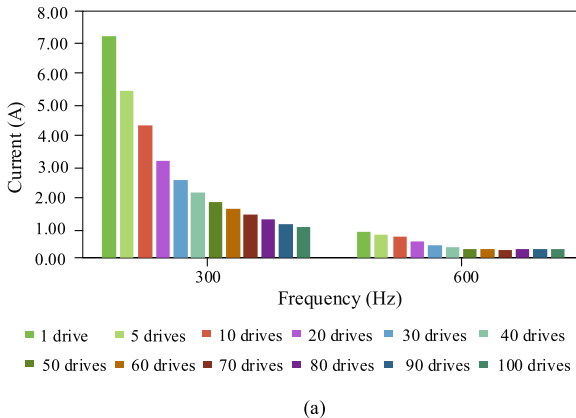
The dc-link capacitor current spectra of scalable standard and slim drives under a soft grid condition are shown in Fig. 14(a) and (b), respectively. The following can be observed from the current spectrum:

- 1) with more standard drives connected in parallel, the current of the dc-link capacitor decreases, which is due to the increase in impedance of the multiple standard drive with the increase in the number of standard drive;
- 2) with more slim drives connected in parallel, the current component of the dc-link capacitor mainly appears at 300 Hz;
- 3) the largest current component in 1, 5, 10, and 30 slim drives appears at 1800, 900, 600, and 300 Hz, respectively, the reason for the large current component is that the resonant frequency of 1, 5, 10, and 30 slim drives are close to 1800, 900, 600, and 300 Hz, respectively; the obtained dc-link capacitor current spectrum is in accordance with impedance characteristics analysis.

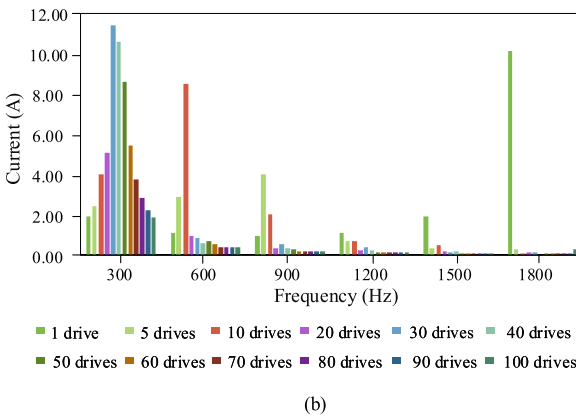
The estimated lifetimes of the dc-link capacitor in multiple standard and slim ASDs under the soft grid condition are shown in Fig. 15(a) and (b), respectively. The following can be obtained:

- 1) considering that the number of standard drives increases from 1 to 100, the B1 lifetime of the dc-link capacitor is extended from 4.4 to 8.0 years;
- 2) the B1 lifetime of 30 slim ASDs is 4.3 years, which is the shorest B1 lifetime of multiple slim ASDs, that is because the current of the dc-link capacitor in the 30 slim drives system at 300 Hz is the highest.

In order to analyze the influence of drive numbers on the dc-link capacitor lifetime more intuitively, the B1 lifetime versus drive numbers curve is shown in Fig. 16 (a) and (b), in which



(a)



(b)

Fig. 14. DC-link capacitor current spectrum with scalable numbers of drives. (a) DC-link capacitor current spectrum of scalable standard drives under soft grid conditions. (b) DC-link capacitor current spectrum of scalable slim drives under soft grid conditions.

different ambient temperature is considered. The following can be seen:

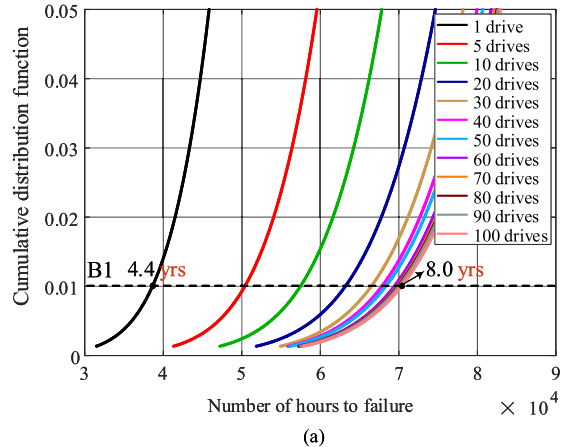
- 1) the B1 lifetime of multiple ASDs at same configurations becomes lower with higher ambient temperature, and the tendency of the capacitor B1 lifetime with drives number is the same at different ambient temperature;
- 2) the B1 lifetime of multiple slim ASDs changes regularly when the number of drives is greater than 30, and the B1 lifetime of ten slim drives is relatively small, as the impedance of ten slim drives at 600 Hz is the smallest.

With the accumulated failure, at five years lifetime, of the multiple drives system, shown in Fig. 17, the following can be seen:

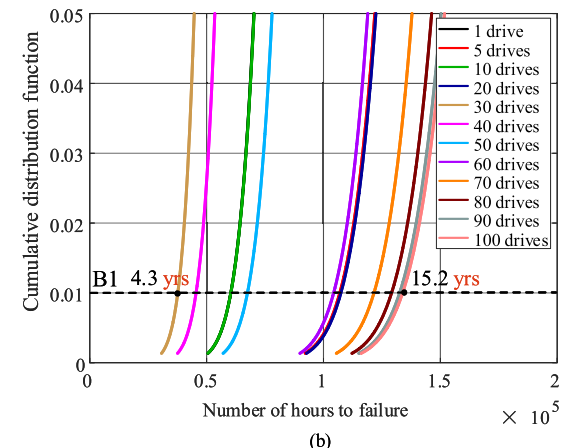
- 1) the accumulated failure at five years lifetime of standard drives decreases with the increase of drives number, and the accumulated failure at five years lifetime of one standard drive is higher than 1%;
- 2) the accumulated failure at five years lifetime of slim drives is less than 1% except 30- and 40-drives systems.

C. Lifetime Prediction of DC-Link Capacitors With Scalable Grid Conditions

The reliability of the dc-link capacitor in multiple drives is mainly determined by the impedance of the ASDs system, and



(a)



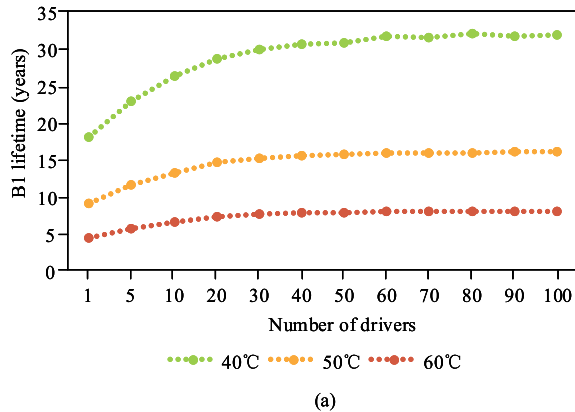
(b)

Fig. 15. Lifetime estimation of dc-link capacitor in multiple standard and slim ASDs under a soft grid condition ($L_g = 130 \mu\text{H}$). (a) Lifetime estimation of dc-link capacitor in multiple standard ASDs under soft grid conditions. (b) Lifetime estimation of dc-link capacitor in multiple slim ASDs under soft grid conditions.

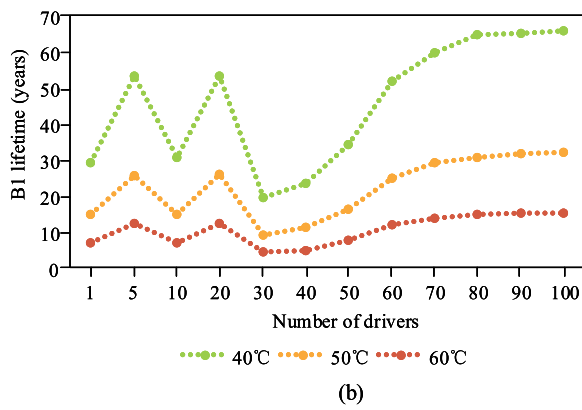
the grid condition is one of the factors that influence the system impedance. Therefore, the impact of grid conditions on the reliability of multiple drives system is studied in this section. The results in Section IV-B show that the reliability of 30 slim drives is the lowest, therefore, the reliability of the dc-link capacitor in 30 standard and slim drives with scalable grid conditions is studied in this section.

With the impedance characteristics of 30 standard and slim ASDs under scalable grid conditions, shown in Fig. 18(a) and (b), respectively, the following can be observed:

- 1) as the grid impedance increases from 1 to 200 μH , the impedance of 30 standard ASDs increases when the frequency is greater than 200 Hz, due to which the current of the dc-link capacitor in the 30 standard drives system decreases with the grid impedance increases;
- 2) when the grid impedance is 10 μH , the impedance of 30 slim ASDs at 900 and 1200 Hz is the smallest, which will result in the largest dc-link capacitor current component at 900 and 1200 Hz;
- 3) when the grid impedance is 50 μH , the impedance of 30 slim ASDs at 600 Hz is the smallest, which will



(a)



(b)

Fig. 16. B1 lifetime of multiple drives system versus drive numbers with different ambient temperature. (a) B1 lifetime of dc-link capacitor in multiple standard drives under soft grid and scalable ambient temperature. (b) B1 lifetime of the dc-link capacitor in multiple slim drives under soft grid and scalable ambient temperature.

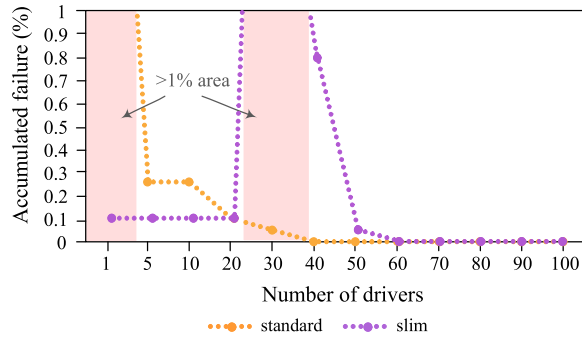
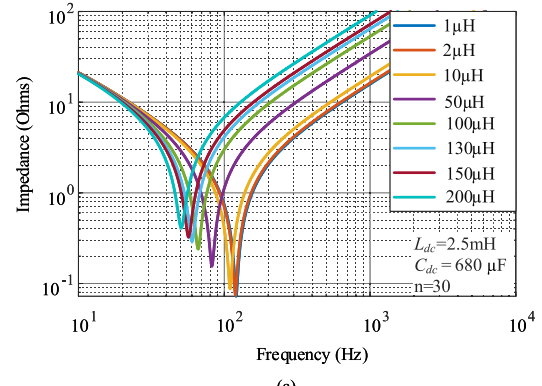


Fig. 17. Accumulated failure at five years lifetime of multiple drives system versus drive numbers.

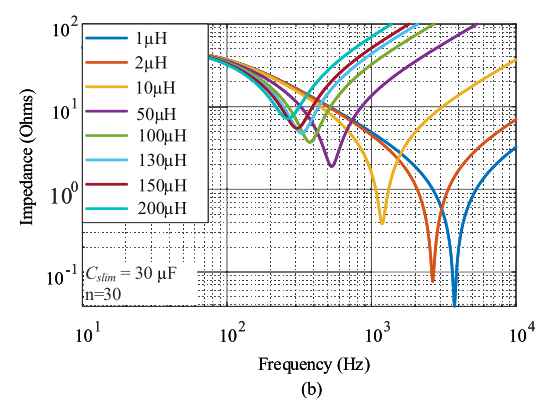
result in the largest dc-link capacitor current component at 600 Hz;

- 4) when the grid impedance is 130 and 150 μH , the impedance of 30 slim ASDs at 300 Hz is the smallest, which will result in the largest dc-link capacitor current component at 300 Hz.

The dc-link capacitor current spectra of 30 standard and slim ASDs under scalable grid conditions are shown in Fig. 19(a).



(a)



(b)

Fig. 18. Impedance characteristics of multiple ASDs system under scalable grid conditions. (a) Impedance characteristics of 30 standard ASDs under scalable grid conditions. (b) Impedance characteristics of 30 slim ASDs under scalable grid conditions.

and (b), respectively. The following can be seen from the current spectrum:

- 1) as the grid impedance increases from 1 to 200 μH , the current of the dc-link capacitor in 30 standard ASDs decreases;
- 2) the current of the dc-link capacitor in 30 slim ASDs mainly appears at 300 Hz, and the largest current component at 300, 600, 900, and 1200 Hz are in accordance with the analysis in impedance characteristics.

With the estimated lifetime of the dc-link capacitor in 30 standard and slim ASDs under scalable grid conditions, shown in Fig. 20(a) and (b), respectively, the following can be obtained:

- 1) as the grid impedance increases from 1 to 200 μH , the B1 lifetime of the dc-link capacitor in 30 standard ASDs is extended from 4.0 to 7.8 years, which is due to the decrease in electrothermal stress of the 30 standard drives system with the increase in grid impedance;
- 2) when the grid impedance is 130- and 150- μH , the B1 lifetime of 30 slim ASDs is 4.3 years, which is the shortest B1 lifetime, that is because the electrothermal stress of 30 slim ASDs with 130- and 150- μH grid configurations is the largest;
- 3) when the grid impedance is 1- μH , the B1 lifetime of 30 slim ASDs is 15.2 years, which is the longest B1 lifetime, that is because the electrothermal stress of 30 slim ASDs with 1- μH grid configurations is the smallest.

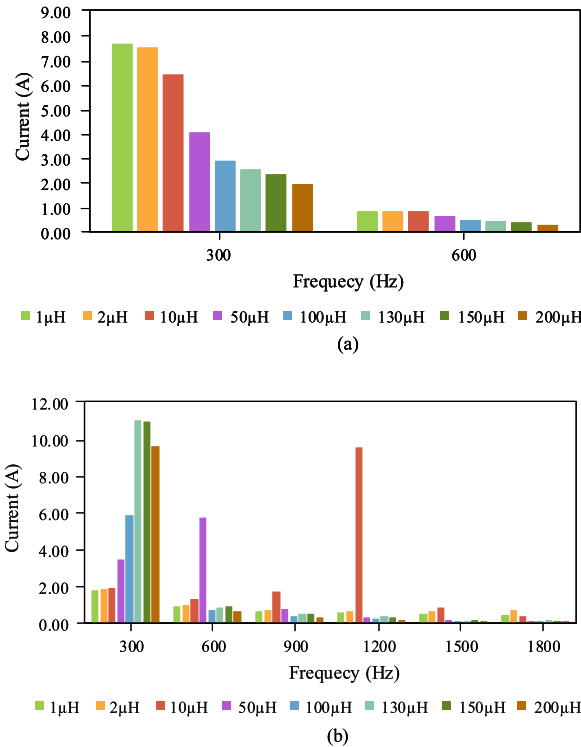


Fig. 19. DC-link capacitor current spectrum under scalable grid conditions. (a) DC-link capacitor current spectrum of 30 standard drives under scalable grid conditions. (b) DC-link capacitor current spectrum of 30 slim drives under scalable grid conditions.

With the B1 lifetime versus grid impedance curve is shown in Fig. 21, the following can be seen:

- 1) the B1 lifetime of the capacitor in 30 standard ASDs extend when the grid impedance becomes larger;
- 2) as the grid impedance increases from 1 μH to 200 μH , the B1 lifetime of the capacitor in 30 slim ASDs fluctuates, which is determined by the ASDs impedance characteristics;
- 3) the B1 lifetime in 30 slim ASDs is longer than that of in 30 standard standard ASDs when the grid impedance is less than 100 μH .

With the accumulated failure at five years lifetime of the multiple drives system is shown in Fig. 22, the following can be observed:

- 1) the accumulated failure at five years lifetime of 30 standard drives decreases with the increase of grid impedance;
- 2) the accumulated failure at five years lifetime of 30 slim drives is less than 1% except in 130- and 150- μH grid configurations.

D. Lifetime Prediction of DC-Link Capacitors in a Hybrid ASDs System

This section studies the lifetime of dc-link capacitors in a hybrid ASDs system with multiple standard and slim drives. From the aforementioned section, it can be seen that the dc-link capacitor in 30 slim drives under soft grid has worse reliability compared with other numbers of slim drives, which is mainly

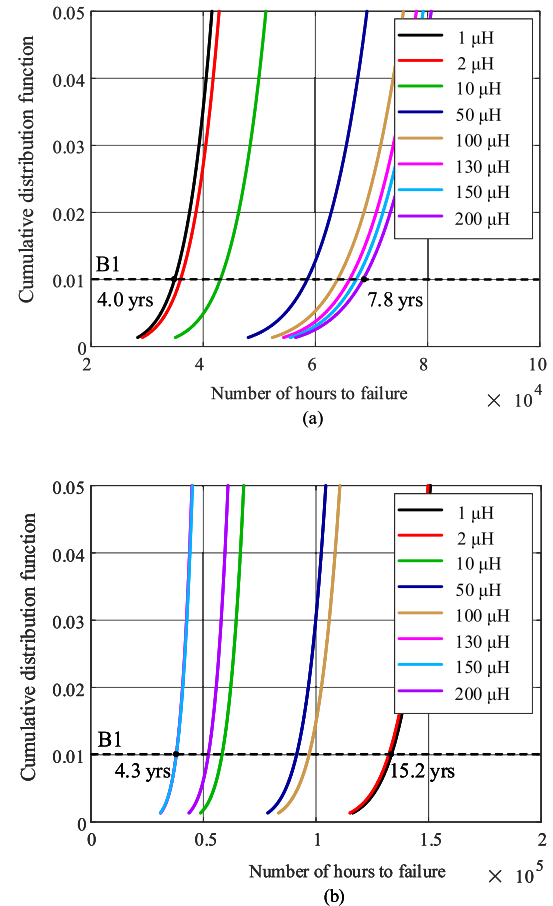


Fig. 20. Lifetime estimation of dc-link capacitor in 30 standard and slim ASDs under scalable grid conditions. (a) Lifetime estimation of dc-link capacitor in 30 standard ASDs under scalable grid conditions. (b) Lifetime estimation of dc-link capacitor in 30 slim ASDs under scalable grid conditions.

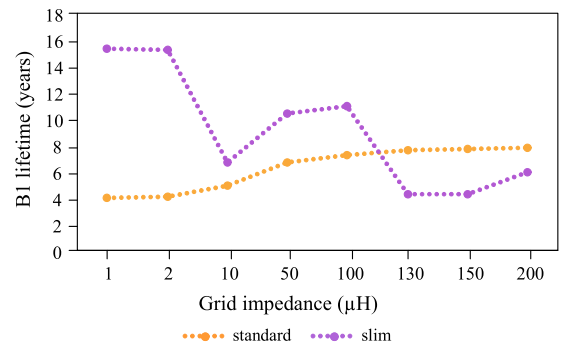


Fig. 21. B1 lifetime of 30 drives system versus grid impedance.

because the resonant frequency of the 30 slim drives system is close to 300 Hz. As a further research, the hybrid drives system studied in this section focuses on the following two scenarios: keep the total number of drives unchanged (e.g., 30) and increase the number of standard drive; and keep the number of slim drives unchanged (e.g., 30) and increase the number of standard drive.

1) *Constant Total Number of Hybrid Drives:* In this section, the total number of hybrid drives is kept constant, while the

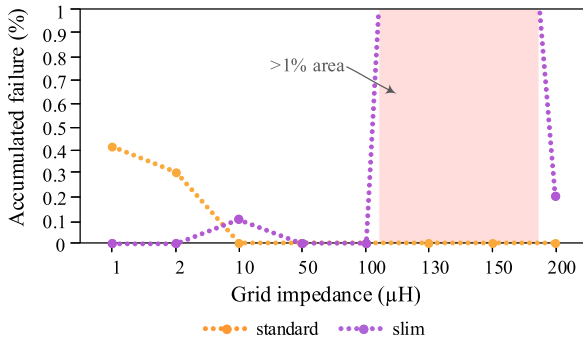


Fig. 22. Accumulated failure at 5 years lifetime of 30 drives system versus grid impedance.

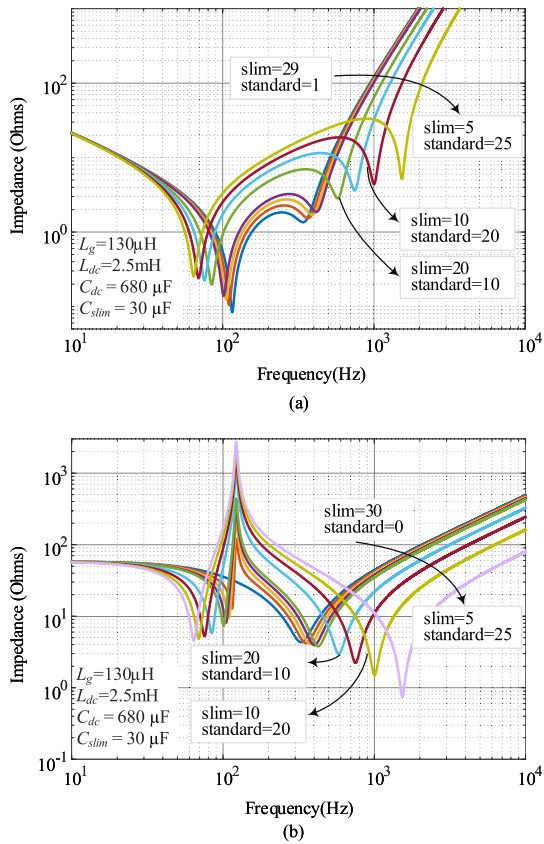


Fig. 23. Impedance characteristics of standard drive and slim drive in a hybrid ASDs system under soft grid conditions. Keep the total number of drives to 30 and increase the percentage of the standard drive. (a) Impedance characteristics of standard drives in hybrid ASDs. (b) Impedance characteristics of slim drives in hybrid ASDs.

hybrid percentage of standard and slim drives varies. With the impedance characteristics of the standard drive and slim drive in a hybrid ASDs system under soft grid conditions are shown in Fig. 23(a) and (b), respectively, in which the total number of drives is kept to 30, the following can be seen:

- 1) with the increase in number of standard drives from 1 to 25, one resonant frequency reduces from 100 to 60 Hz, while the other one increases from 300 to 1000 Hz;
- 2) the resonant frequency of the standard drive and slim drive in the combination of the 20 slim drives and 10 standard drives system is close to 600 Hz, which will result in a

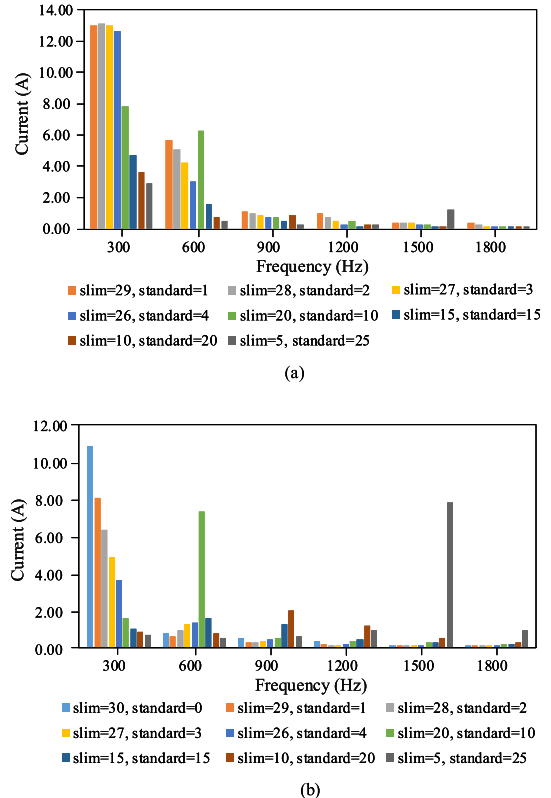


Fig. 24. DC-link capacitor current spectrum of standard drive and slim drive in a hybrid ASDs system under soft grid conditions. Keep the total number of drives to 30 and increase the percentage of the standard drive. (a) DC-link capacitor current spectrum of standard drives in hybrid ASDs system. (b) DC-link capacitor current spectrum of slim drives in hybrid ASDs system.

high dc-link capacitor current at 600 Hz; similarly, the resonant frequency of the standard drive and slim drive in the combination of the 10 slim drives and 20 standard drives system is close to 900 Hz, which results in high dc-link capacitor current at 900 Hz.

The dc-link capacitor current spectra of the standard drive and slim drive in a hybrid ASDs system under soft grid conditions, shown in Fig. 24(a) and (b), respectively. The following can be seen from the current spectrum:

- 1) the current of the dc-link capacitor in standard drive and slim drive mainly appears at 300 and 600 Hz;
- 2) the current component at 600 Hz is the largest when there are 20 slim drives and 10 standard drives, which is because its resonant frequency is close to 600 Hz;
- 3) similarly, the maximum current component at 900, 1200, 1500, and 1800 Hz can be explained in the same way.

With the accumulated failures at 5 years for the standard drive and slim drive in a hybrid ASDs system under soft grid conditions, shown in Fig. 25(a) and (b), respectively. With the following can be seen:

- 1) the accumulated failure at 5 years for standard drives is less than 1% when the number of the standard drive is greater than 15;
- 2) the accumulated failure at 5 years for slim drives is less than 1% when the standard drive is added;

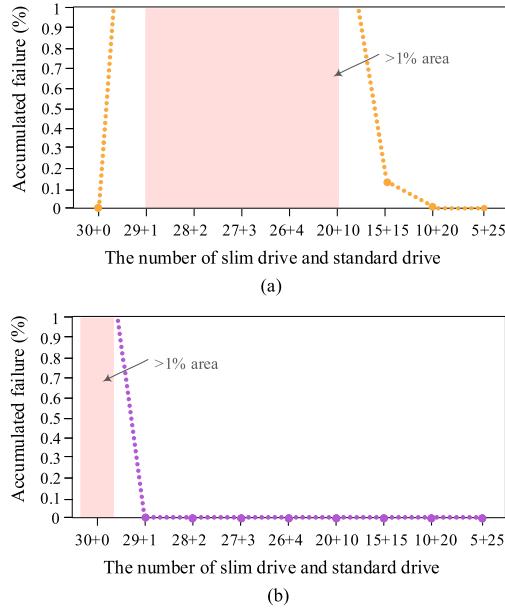


Fig. 25. Accumulated failure at 5 years lifetime of hybrid ASDs system under soft grid conditions. Keep the total number of drives to 30 and increase the percentage of the standard drive.

3) when the total number of drives is kept to 30 and the number of standard drives is increased, the reliability of the slim drive is improved, however, the standard drive has higher reliability only when the number of standard drives reaches to 15.

2) *Constant Number of Slim Drives:* In this section, the number of slim drives keeps constant and the total number increases by adding multiple standard drives. With the impedance characteristics of the standard drive and slim drive in the hybrid ASDs system under soft grid conditions, shown in Fig. 26(a) and (b), respectively, the following can be seen:

- 1) as the number of standard drives increases from 1 to 30, one resonant frequency of the standard drive increases from 300 to 800 Hz, while the other one reduces from 100 to 60 Hz;
- 2) the resonant frequency of the standard drive and slim drive in the combination of the 30 slim drives and 25 standard drives system is close to 600 Hz, which results in a high dc-link capacitor current at 600 Hz;

With the dc-link capacitor current spectrum of the standard and slim hybrid ASDs system under soft grid conditions, shown in Fig. 27(a) and (b), respectively, the following can be seen from the current spectrum:

- 1) the current of the dc-link capacitor in the standard drive and slim drive mainly appears at 300 and 600 Hz;
- 2) the current component at 600 Hz is the largest when the number of drives is the combination of 30 slim drives and 25 standard drives, which is because its resonant frequency is close to 600 Hz;
- 3) similarly, the maximum current component at 900, 1200, 1500, and 1800 Hz can be explained in the same way.

With the accumulated failures at five years for the standard drive and slim drive in a hybrid ASDs system under soft grid

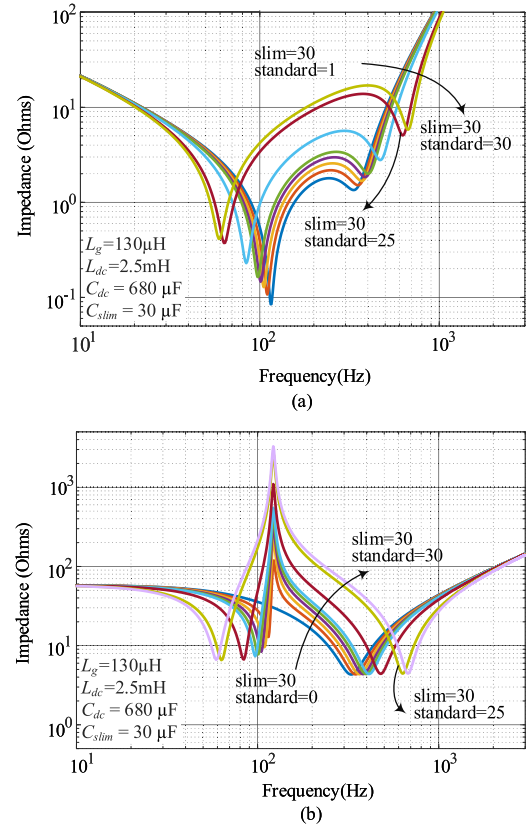


Fig. 26. Impedance characteristics of standard drive and slim drive in hybrid ASDs system under soft grid conditions. Keep the number of slim drives to 30 and increase the number of standard drives. (a) Impedance characteristics of standard drives in hybrid ASDs. (b) Impedance characteristics of slim drives in hybrid ASDs.

conditions, shown in Fig. 28(a) and (b), respectively, in which the number of slim drive is kept to 30, the following can be seen:

- 1) the accumulated failure at five years lifetime of standard drives is less than 1% when the number of standard drives is greater than 25;
- 2) the accumulated failure at five years lifetime of slim drives is less than 1% when standard drives are added;
- 3) when the number of slim drives is kept to 30 and the number of standard drives are increased, the reliability of slim drives is improved, however, the standard drives have higher reliability only when the number of standard drives reaches to 25.

The results of two types of hybrid ASDs systems show that: comparing with the 30 slim drives system, the slim drives in the hybrid ASDs system studied in this section have higher reliability, however, the standard drive meet reliability issue when the number is less than 10.

V. CAPACITOR SIZING OF MULTIDRIVE SYSTEMS CONSIDERING RELIABILITY PERFORMANCE

Section IV investigates the reliability of the dc-link capacitor in a multiple standard and slim ASDs system, and the results show that the reliability of the dc-link capacitor in multiple slim drives is sensitive to the capacitance of the dc-link capacitor

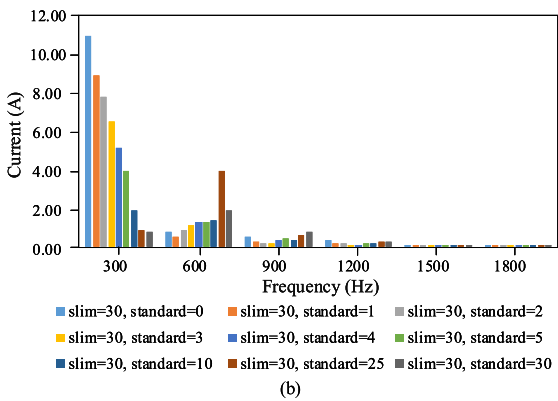
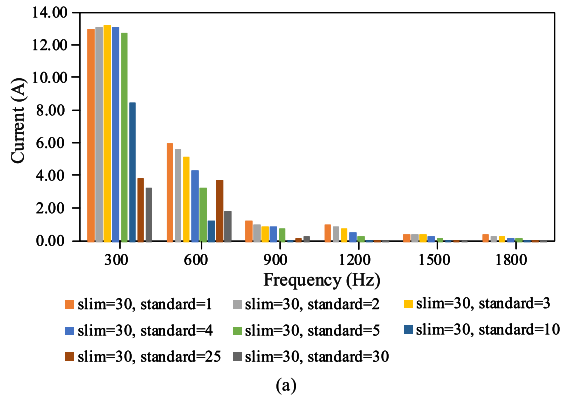


Fig. 27. DC-link capacitor current spectrum of standard drive and slim drive in hybrid ASDs system under soft grid conditions. Keep the number of slim drives to 30 and increase the number of standard drives.

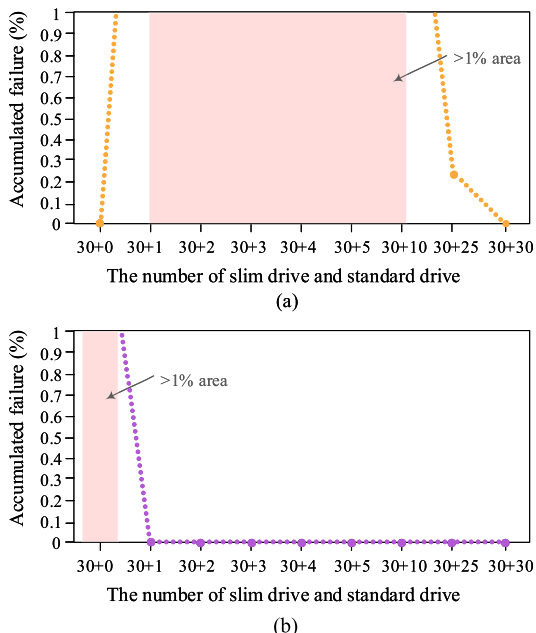


Fig. 28. Accumulated failure at 5 years lifetime of hybrid ASDs system under soft grid conditions. Keep the number of slim drives to 30 and increase the number of standard drives. (a) Accumulated failure at five years lifetime of standard drive. (b) Accumulated failure at five years lifetime of slim drive.

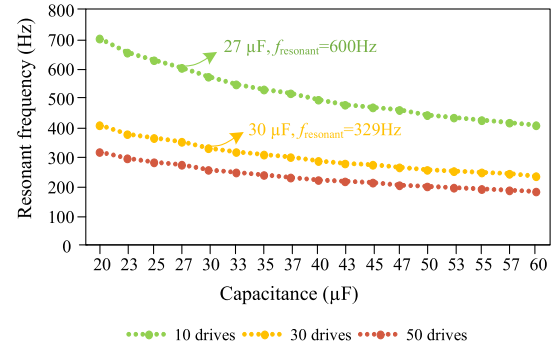


Fig. 29. Relationship between capacitance and resonant frequency of multiple slim drives under soft grid condition using parameters in Table I.

in the scalable numbers of drives and grid impedance. The capacitor sizing for a single ASD from the aspect of power quality has been studied before, however, the study in a multiple slim drives system is rare. Therefore, the capacitor sizing criteria for the multiple slim drives system from the reliability aspect are studied in this section. For the case study, the multiple slim drives system specification is in accordance with parameters shown in Table I. The capacitance ranges from 20 to 60 μF and the relationship curve between capacitance and the resonant frequency of the multiple slim drives system is shown in Fig. 29, where the capacitor sizing criteria in 10, 30, and 50 slim drives from the reliability aspect are investigated. The following can thus be seen from Fig. 29.

- 1) As the capacitance increases from 20 to 60 μF , the resonant frequency decreases from 700 to 180 Hz,
- 2) When ten slim drives are connected in parallel, the resonant frequency decreases from 700 to 400 Hz. Especially at 27 μF , the resonant frequency is 600 Hz, which increases the gain for the 600-Hz ripple;
- 3) When 30 slim drives are connected in parallel, the resonant frequency decreases from 400 to 230 Hz. Especially at 30 μF , the resonant frequency is close to 300 Hz, which increases the gain for the 300-Hz ripple;
- 4) when 50 slim drives are connected in parallel, the resonant frequency decreases from 310 to 180 Hz, so that the larger capacitance values move the resonant frequency away from 300 Hz, which reduces the gain for the 300-Hz ripple.

With the estimated lifetimes of the dc-link capacitor in 10, 30, and 50 slim drives under soft grid condition, shown in Fig. 30(a)–(c), respectively, the following is seen:

- 1) when ten slim drives are connected in parallel, the B1 lifetime of the dc-link capacitor with 27 μF is the shortest (i.e., 4.5 years);
- 2) when 30 slim drives are connected in parallel, the B1 lifetime of the dc-link capacitor with 30 μF is the shortest (i.e., 4.3 years);
- 3) when 50 slim drives are connected in parallel, the B1 lifetime of dc-link capacitor with 20 μF is the shortest (i.e., 1.9 years).

The relationship between the dc-link capacitor B1 lifetime and capacitance under multiple slim drives are irregular, which is inconvenient for the capacitor sizing, as a result, the relationship

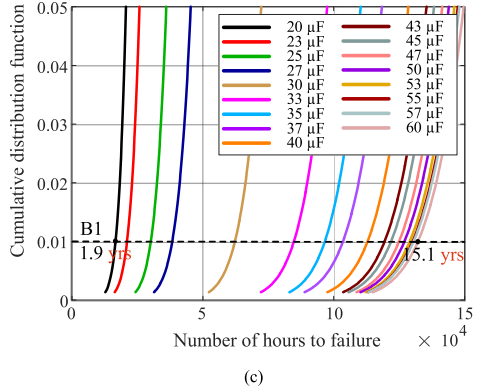
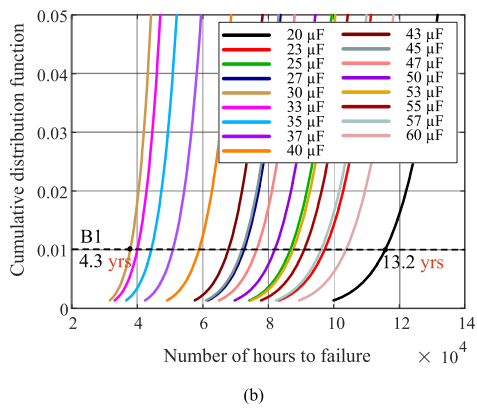
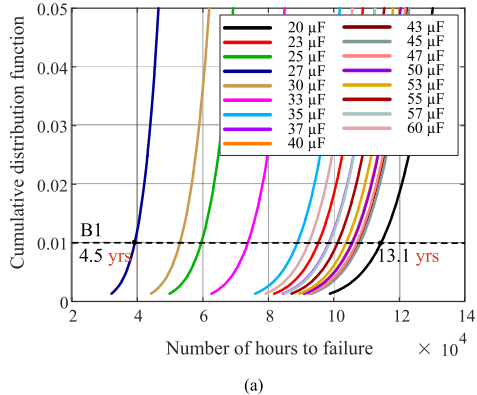


Fig. 30. Lifetime estimation of dc-link capacitor with scalable capacitance in multiple slim drives under a soft grid condition ($L_g = 130 \mu\text{H}$). (a) Lifetime estimation of the dc-link capacitor with scalable capacitance in ten slim ASDs under the soft grid condition. (b) Lifetime estimation of the dc-link capacitor with scalable capacitance in 30 slim ASDs under the soft grid condition. (c) Lifetime estimation of the dc-link capacitor with scalable capacitance in 50 slim ASDs under soft grid condition.

curve between the dc-link capacitor B1 lifetime and capacitance under multiple slim drives are depicted in Fig. 31 showing the following:

- 1) when ten slim drives are connected in parallel, the B1 lifetime of the dc-link capacitor with $27 \mu\text{F}$ is less than 5 years;
- 2) when 30 slim drives are connected in parallel, the B1 lifetime of the dc-link capacitor with $30\text{--}33 \mu\text{F}$ is less than 5 years;

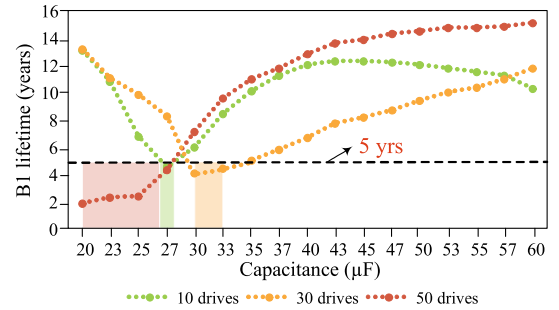


Fig. 31. Relationship between the dc-link capacitor B1 lifetime and capacitance under multiple slim drives.

- 3) when 50 slim drives are connected in parallel, the B1 lifetime of the dc-link capacitor with $20\text{--}27 \mu\text{F}$ is less than 5 years, and the larger the capacitance, the higher the reliability of the dc-link capacitor.

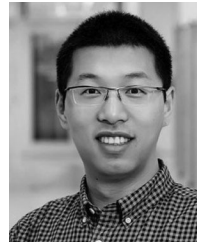
VI. CONCLUSION

This article investigates the lifetime of the dc-link capacitors in multidrive systems. An analytical model to obtain the dc-link continuous current in multiple standard and slim drives is provided, which makes the dc-link capacitor stress analysis away from simulation and becomes easy to modify and optimize. Based on the proposed analytical model and the lifetime prediction method, the relationship between the dc-link capacitor lifetime and the configurations of the multidrive systems in terms of structures, numbers of drive, and grid conditions is found. It quantifies the impact of drive numbers and grid conditions, which should be considered in the concept and design phase of multiple ASDs. Based on the case study with the presented specification, the following conclusions can be drawn.

- 1) In multiple standard drives, the B1 lifetime of the dc-link capacitor extend with more drives connected in parallel at the PCC, while in multiple slim drives, the B1 lifetime of the dc-link capacitor in 30 slim drives is the shortest.
- 2) The B1 lifetime of the dc-link capacitor in 30 standard drives extend with larger grid impedance, while in 30 slim drives, the B1 lifetime of dc-link capacitor is the shortest when the grid impedance is 130 and $150 \mu\text{H}$.
- 3) The reliability of the dc-link capacitor in a slim drive is improved by adding standard drives to the ASDs system, however, the reliability of the standard drive in a hybrid ASDs system is worse, unless the standard drive reaches to a certain number.
- 4) From the reliability point of view, when multiple drives are in soft grid and heavy load condition, the value of the capacitor in a ten slim drives system grid should be selected other than $27 \mu\text{F}$; for the 30 slim drives system, the value of the capacitor should be selected other than $30\text{--}33 \mu\text{F}$; for the 50 slim drives system, the value of the capacitor should be selected larger than $27 \mu\text{F}$ in order to keep lifetime longer than 5 years in the studied case.

REFERENCES

- [1] H. Wang, P. Davari, H. Wang, and D. Kumar, "Lifetime estimation of DC-link capacitors in adjustable speed drives under grid voltage unbalances," *IEEE Trans. Power Electron.*, vol. 34, no. 5, pp. 4064–4078, May. 2019.
- [2] F. Zare, H. Soltani, D. Kumar, and P. Davari, "Harmonic emissions of three-phase diode rectifiers in distribution networks," *IEEE Access*, vol. 5, pp. 2819–2833, 2017.
- [3] H. Wang and F. Blaabjerg, "Reliability of capacitors for DC-Link applications in power electronic converters—An overview," *IEEE Trans. Ind. Appl.*, vol. 50, no. 5, pp. 3569–3578, Sep. 2014.
- [4] H. Wang, M. Liserre, and F. Blaabjerg, "Toward reliable power electronics—Challenges design tools and opportunities," *IEEE Ind. Electron. Mag.*, vol. 70, no. 2, pp. 17–26, Jun. 2013.
- [5] S. Yang, A. Bryant, P. Mawby, D. Xiang, L. Ran, and P. Tavner, "An industry-based survey of reliability in power electronic converters," in *Proc. IEEE Energy Convers. Congr. Expo.*, 2009, pp. 3151–3157.
- [6] M. A. Vogelsberger, T. Wiesinger, and H. Ertl, "Life-cycle monitoring and voltage-managing unit for DC-Link electrolytic capacitors in PWM converters," *IEEE Trans. Power Electron.*, vol. 26, no. 2, pp. 493–503, Feb. 2011.
- [7] K. S. Rajashekara, V. Rajagopalan, A. Sevigny, and J. Vithayathil, "DC-link filter design considerations in three-phase voltage source inverter-fed induction motor drive system," *IEEE Trans. Ind. Appl.*, vol. 23, no. 4, pp. 673–680, Jul. 1987.
- [8] D. Kumar, P. Davari, F. Zare, and F. Blaabjerg, "Analysis of three-phase rectifier systems with controlled dc-link current under unbalanced grids," in *Proc. IEEE Appl. Power Electron. Conf. Expo.*, 2017, pp. 2179–2186.
- [9] V. Dzankhotov and J. Pyrhnen, "Passive LC filter design considerations for motor applications," *IEEE Ind. Electron. Mag.*, vol. 60, no. 10, pp. 4253–4259, Oct. 2013.
- [10] H. Wang and H. Wang, "Performance evaluation of a two-terminal active inductor in the DC-link filter of a three-phase diode bridge rectifier," in *Proc. IEEE Appl. Power Electron. Conf. Expo.*, 2019, pp. 2844–2848.
- [11] H. Wang, H. Wang, G. Zhu, and F. Blaabjerg, "An overview of capacitive DC links—Topology derivation and scalability analysis," *IEEE Trans. Power Electron.*, vol. 43, no. 2, pp. 495–504, Mar. 2007.
- [12] M. Hinkkanen and J. Luomi, "Induction motor drives equipped with diode rectifier and small DC-Link capacitance," *IEEE Trans. Ind. Electron.*, vol. 55, no. 1, pp. 312–320, Jan. 2008.
- [13] H. M. Delpino and D. Kumar, "Line harmonics on systems using reduced DC-link capacitors," in *Proc. IEEE 39th Annu. Conf. IEEE Ind. Electron. Soc.*, 2013, pp. 961–966.
- [14] M. F. Firuzi, A. Roosta and M. Gitizadeh, "Stability analysis and decentralized control of inverter-based ac microgrid," *Protection Control Modern Power Syst.*, vol. 4, no. 6, pp. 1–24, Dec. 2019.
- [15] H. Akagi, "Active harmonic filters," *Proc. IEEE*, vol. 93, no. 12, pp. 2128–2141, Dec. 2005.
- [16] J. C. Das, "Passive filters—Potentialities and limitations," *IEEE Trans. Ind. Electron.*, vol. 40, no. 1, pp. 232–241, Jan. 2004.
- [17] H. Wen, W. Xiao, X. Wen, and P. Armstrong, "Analysis and evaluation of DC-link capacitors for high-power-density electric vehicle drive systems," *IEEE Trans. Veh. Technol.*, vol. 61, no. 7, pp. 2950–2964, Sep. 2012.
- [18] Y. Yang, K. Ma, H. Wang, and F. Blaabjerg, "Instantaneous thermal modeling of the DC-link capacitor in photovoltaic systems," in *Proc. IEEE Appl. Power Electron. Conf. Expo.*, 2015, pp. 2733–2739.
- [19] H. Wang and H. Wang, "Benchmark of DC-link LC filters based on passive inductor and two-terminal active inductor," in *Proc. IEEE Int. Conf. Ind. Technol.*, 2019, pp. 388–393.
- [20] M. Chen, H. Wang, H. Wang, F. Blaabjerg, X. Wang, and D. Pan, "Reliability assessment of hybrid capacitor bank using electrolytic- and film-capacitors in three-level neutral-point-clamped inverters," in *Proc. IEEE Appl. Power Electron. Conf. Expo.*, 2019, pp. 2826–2832.
- [21] B. K. Bose, "Power electronics and motor drives recent progress and perspective," *IEEE Trans. Ind. Electron.*, Feb. 2009, vol. 56, no. 2, pp. 581–588.
- [22] H. Saren, O. Pyrhonen, K. Rauma, and O. Laakkonen, "Overmodulation in voltage source inverter with small DC-link capacitor," in *Proc. IEEE Power Electron. Specialists Conf.*, 2005, pp. 892–898.
- [23] H. Wang, P. Davari, D. Kumar, and F. Zare, "The impact of grid unbalances on the reliability of DC-link capacitors in a motor drive," in *Proc. IEEE Energy Convers. Congress Expo.*, 2017, pp. 4345–4350.
- [24] H. Wang, P. Davari, H. Wang, and D. Kumar, "Lifetime benchmarking of two DC-link passive filtering configurations in adjustable speed drives," in *Proc. IEEE Appl. Power Electron. Conf. Expo.*, 2018, pp. 228–233.
- [25] F. Zare, "Harmonics issues of three-phase diode rectifiers with a small DC-link capacitor," in *Proc. IEEE Int. Power Electron. Motion Control Conf. Expo.*, 2014, pp. 912–917.
- [26] M. Sakui, H. Fujita, and M. Shioya, "A method for calculating harmonic currents of a three-phase bridge uncontrolled rectifier with DC filter," *IEEE Trans. Ind. Electron.*, vol. 36, no. 3, pp. 434–440, Aug. 1989.



Haoran Wang (Member, IEEE) received the B.S. and M.S. degrees in control science and engineering from the Wuhan University of Technology, Wuhan, China, in 2012 and 2015, respectively, and the Ph.D. degree in power electronics from the Center of Reliable Power Electronics, Aalborg University, Aalborg, Denmark, in 2018.

He is currently an Assistant Professor with Aalborg University. From July 2013 to September 2014, he was a Research Assistant with the Department of Electrical Engineering, Tsinghua University, Beijing, China. He was a Visiting Scientist with the ETH Zurich, Switzerland, from December 2017 to April 2018. His research interests include capacitors in power electronics, reliability of power electronic systems, and multiobjective life-cycle performance optimization of power electronic systems.



Shili Huang (Student Member) received the B.S. degree in electrical engineering from the Hubei University of Technology, Wuhan, China, in 2017. She is currently working toward the master's degree in electrical engineering with the Wuhan University of Technology, Wuhan.

Her research interests include capacitors in power electronics, reliability of power electronic systems, and dc-link capacitors.



Dinesh Kumar (Senior Member, IEEE) received the M.Tech. degree in power system engineering from the Indian Institute of Technology, Roorkee, India, in 2004, and the Ph.D. degree in power electronics from the University of Nottingham, Nottingham, U.K., in 2010.

From 2004 to 2005, he served as a Lecturer with Electrical Engineering Department, National Institute of Technology, Kurukshetra, India. In 2006, he joined Technical University Chemnitz, Chemnitz, Germany as a Research Fellow in power electronics. From 2006 to 2010, he investigated and developed the matrix converter-based multidrive system for aerospace applications. Since 2011, he has been with the Danfoss Drives A/S, Grasten, Denmark, where he is involved in many research and industrial projects. His current research interests include motor drive, harmonic analysis and mitigation techniques, power quality, and electromagnetic interference in power electronics.

Dr. Kumar is a member of the IEC Standardization Working Group in TC77A and SyC LVdc committee. He is the Editor-in-Chief for the *International Journal of Power Electronics* and the Associate Editor for the IEEE TRANSACTION ON INDUSTRY APPLICATIONS and IEEE ACCESS JOURNAL.



Qian Wang (Member, IEEE) was born in Hubei Province, China, in 1990. She received the bachelor's degree in electrical engineering from the Wuhan University of Technology, Wuhan, China, in 2012, the master's degree in high voltage engineering from the Huazhong University of Science and Technology, Wuhan, in 2015, and the Ph.D. degree in high voltage engineering from the Department of Energy Technology, Aalborg University, Aalborg, Denmark, in 2018.

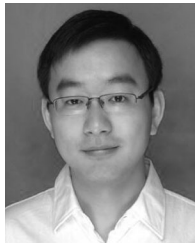
She is currently an Assistant Professor with Aalborg University. Her research interests include electrical design / testing of innovative, composite-based transmission towers, and insulation in modern power electronic components.



Huai Wang (Senior Member, IEEE) received the B.E. degree in electrical engineering, from the Huazhong University of Science and Technology, Wuhan, China, in 2007, and the Ph.D. degree in power electronics from the City University of Hong Kong, Hong Kong, in 2012.

He is currently a Professor with the Center of Reliable Power Electronics, Aalborg University, Aalborg, Denmark. He was a Visiting Scientist with the ETH Zurich, Switzerland, from August to September 2014, and with the Massachusetts Institute of Technology, Cambridge, MA, USA, from September to November 2013. He was with the ABB Corporate Research Center, Switzerland, in 2009. His research interests include the fundamental challenges in modeling and validation of power electronic component failure mechanisms, and application issues in system-level predictability, condition monitoring, circuit architecture, and robustness design.

Dr. Wang was the recipient of the Richard M. Bass Outstanding Young Power Electronics Engineer Award from the IEEE Power Electronics Society in 2016, and the Green Talents Award from the German Federal Ministry of Education and Research in 2014. He is currently the Award Chair of the Technical Committee of the High Performance and Emerging Technologies, IEEE Power Electronics Society, and the Chair of IEEE PELS/IAS/IE Chapter in Denmark. He serves as an Associate Editor for the *IET Power Electronics*, IEEE JOURNAL OF EMERGING AND SELECTED TOPICS IN POWER ELECTRONICS, and IEEE TRANSACTIONS ON POWER ELECTRONICS.



Xiangtian Deng (Member, IEEE) received the B.E. degree from China Three Gorges University, Yichang, China, in 2005, and the Ph.D. degree from Wuhan University, Wuhan, China, in 2015, both in electrical engineering.

Since 2015, he has been a Faculty Member with Wuhan University of Technology, Wuhan, where he is currently working as an Associate Professor with the School of Automation. His research interest includes the control and protection of dc microgrids, and active capacitors.



Guorong Zhu (Senior Member, IEEE) was born in Hunan, China. She received the Ph.D. degree in electrical engineering from the Huazhong University of Science and Technology, Wuhan, China, in 2009.

From 2002 to 2005, she was a Lecturer with the School of Electrical Engineering, Wuhan University of Science and Technology, Wuhan. From 2009 to 2011, she was a Research Assistant/Research Associate with the Department of Electronic and Information Engineering, The Hong Kong Polytechnic University, Hong Kong. From 2016 to 2017, she was a Visiting Scholar with the Department of Energy Technology, Aalborg University, Aalborg, Denmark. She is currently an Associate Professor with the School of Automation, Wuhan University of Technology, Wuhan. Her research interests include power electronics equipment reliability, battery energy storage technology, and wireless power transfer technology.